

# Large deviations in statistics of the convex hull of passive and active particles: A theoretical study

Soheli Mukherjee<sup>1,\*</sup> and Naftali R. Smith<sup>1,†</sup>

<sup>1</sup>*Department of Environmental Physics, Blaustein Institutes for Desert Research,  
Ben-Gurion University of the Negev, Sede Boqer Campus, 8499000, Israel*

We investigate analytically the distribution tails of the area  $A$  and perimeter  $L$  of a convex hull for different types of planar random walks. For  $N$  noninteracting Brownian motions of duration  $T$  we find that the large- $L$  and  $A$  tails behave as  $\mathcal{P}(L) \sim e^{-b_N L^2/D^T}$  and  $\mathcal{P}(A) \sim e^{-c_N A/D^T}$ , while the small- $L$  and  $A$  tails behave as  $\mathcal{P}(L) \sim e^{-d_N DT/L^2}$  and  $\mathcal{P}(A) \sim e^{-e_N DT/A}$ , where  $D$  is the diffusion coefficient. We calculated all of the coefficients ( $b_N, c_N, d_N, e_N$ ) exactly. Strikingly, we find that  $b_N$  and  $c_N$  are independent of  $N$ , for  $N \geq 3$  and  $N \geq 4$ , respectively. We find that the large- $L$  ( $A$ ) tails are dominated by a single, most probable realization that attains the desired  $L$  ( $A$ ). The left tails are dominated by the survival probability of the particles inside a circle of appropriate size. For active particles and at long times, we find that large- $L$  and  $A$  tails are given by  $\mathcal{P}(L) \sim e^{-T\psi_N^{\text{per}}(L/T)}$  and  $\mathcal{P}(A) \sim e^{-T\psi_N^{\text{rea}}(\sqrt{A}/T)}$  respectively. We calculate the large deviation functions  $\Psi_N$  exactly and find that they exhibit multiple singularities. We interpret these as dynamical phase transitions of first order. We extended several of these results to dimensions  $d > 2$ . Our analytic predictions display excellent agreement with existing results that were obtained from extensive numerical simulations.

## I. INTRODUCTION

### A. Background

Brownian motion is a fundamental stochastic process that appears in many systems ranging from biology, physics, finance, computer science and many more [1]. Brownian motion represents a broad universality class in the sense that for many models of random walks (RWs) and/or models of active particles – particles that generate dissipative, persistent motion by extracting energy from their surroundings [2–6] – the long-time typical behavior converges to that of a Brownian (passive) particle. Examples of active matter arise in many biological systems like cellular tissue behaviour [7], bacterial motion [8, 9], formation of fish schools [10] and many more. Active particles exhibit a wide range of interesting behaviour like non-Boltzmann stationary state [11, 12], clustering at boundaries [13], jamming [14] etc. Different models of RWs and/or active particles are used to model various realistic systems such as movement of animals, self propelled particles, polymers etc.

The convex hull of a trajectory is the minimal convex set that contains all of the points along the trajectory. Convex hulls of stochastic trajectories have attracted much recent interest and they find many applications. For instance, they provide a natural way to define the home range of animals, which is the territory that the animal covers during a certain period of time. The area and perimeter of the convex hull thus gives a quantitative measurement of the home range [15, 16]. Apart from the home range, the convex hull is a useful tool for analyzing

other phenomena, for instance to detect different phases in intermittent stochastic trajectories [17], or to study the spread of animal epidemics [18].

The mean perimeter and area of convex hull of a random walk as a function of number of steps  $t$  is known (in the limit of large number of steps where it converges to Brownian motion) [19]. In the large  $t$  limit, the mean perimeter and area scale as  $\langle L \rangle \sim \sqrt{t}$  and  $\langle A \rangle \sim t$  respectively. These results have been extended to many systems in the literature of physics [20–29] and mathematics [30–32]. For example: Using the connection to extreme value statistics, exact results have been obtained for the mean perimeter and mean area for the convex hull of  $N$  noninteracting planar Brownian motions [20, 21]. In addition, the mean volume and surface area of the convex hull in arbitrary dimensions  $d$  has been calculated for a single Brownian motion and Brownian bridge [30–32], Lévy processes [33], and a single Brownian motion in a confined geometry [34].

Analytical calculations of the variance and higher order moments of the distribution of these quantities are difficult [35]. To our knowledge, the only case for which an analytic result exists for the higher moments is for Brownian bridges [36], which is a Brownian motion constrained to end at its starting point. It is also called a “closed” Brownian motion (in contrast with the unconstrained “open” Brownian motion).

In contrast, extensive numerical studies of the properties of convex hulls have been performed. These studies investigated not only the regime of typical fluctuations, but also used advanced importance-sampling techniques to probe far into the large-deviation regimes, describing convex hulls that are much larger or much smaller than average. The full distributions of the observables like area ( $A$ ) and perimeter ( $L$ ) in  $d = 2$  dimensions, as well as their extensions to higher dimensions volume ( $V$ ) and surface area ( $\mathcal{A}$ ) have been numerically computed

\* soheli.mukherjee2@gmail.com

† naftalismsmith@gmail.com

for different types of stochastic processes. These include the single planar Brownian motion or bridge [22], multiple Brownian motions [23], Brownian motion in higher dimensions [24], self avoiding random walk [25, 26], run and tumble particle [27], Brownian motion with resetting [28]. These numerical simulations were able to calculate the atypical fluctuations with probabilities that are in some cases extremely small, of order  $10^{-1000}$  or even less. However, a comprehensive theory describing these numerical results is still lacking. Analytically there has been partial recent progress in mathematical literature for the ‘right’ tails for the perimeter and area of a single random walker (under certain assumptions) [37, 38].

In this paper, we calculate exactly the distribution of the tails of  $A$ ,  $L$ ,  $V$  and  $\mathcal{A}$  for different types of stochastic processes. We consider both passive and active particles. We find that the physical picture in the right and left tails of the distributions is markedly different. As shown below, the right tails are dominated by a single, optimal large-scale trajectory of the process. In contrast, the left tails are dominated by realizations of the process that remain within a circle of appropriate size. The understanding of these physical pictures is what enables us to obtain the distribution tails analytically.

## B. Model definitions

Let us now define precisely the theoretical models for which we aim to study the convex-hull area and perimeter distributions.

- **Brownian motion.** The motion of a Brownian particle in arbitrary dimension is described by the following Langevin equation:

$$\dot{\mathbf{r}}(t) = \sqrt{2D} \boldsymbol{\xi}(t) \quad (1)$$

where  $\mathbf{r}(t)$  is the position of the particle at time  $t$  and  $0 < t < T$ ,  $D$  is the diffusion constant and  $\boldsymbol{\xi}(t)$  are Gaussian white noises with  $\langle \boldsymbol{\xi}(t) \rangle = 0$  and  $\langle \xi_i(t) \xi_j(t') \rangle = \delta_{ij} \delta(t - t')$ . Here  $\langle \cdot \rangle$  denotes the ensemble average over realizations of the noise.

In  $d = 2$ , dimensional analysis yields the following scaling relations of the perimeter and the area distribution in the physical parameters (i.e  $L$ ,  $A$ ,  $D$  and  $T$ ) [22]

$$\mathcal{P}(L) = \frac{1}{\sqrt{DT}} P\left(\frac{L}{\sqrt{DT}}\right) \quad (2)$$

$$\mathcal{P}(A) = \frac{1}{DT} P\left(\frac{A}{DT}\right) \quad (3)$$

where the functions  $P$  and their arguments are dimensionless.

- **Active particles.** A generic theoretical model for active particles can be written as

$$\dot{\mathbf{r}}(t) = \boldsymbol{\Sigma}(t) \quad (4)$$

where  $\boldsymbol{\Sigma}(t)$  represents a noise term that originates in the self-propulsion of the particle with correlation time  $1/\tau$ . While most of our investigations for active particles will be quite general (under fairly mild assumptions as detailed below), for the sake of concreteness we will also give explicit results for particular models. Two of the most extensively studied models in  $d = 2$  are: Active Brownian particle (ABP) [39] with the following equation of motion

$$\dot{x} = v_0 \cos \theta(t), \quad \dot{y} = v_0 \sin \theta(t), \quad \dot{\theta} = \sqrt{2D_r} \eta(t) \quad (5)$$

where  $\eta(t)$  is a Gaussian white noise with  $\langle \eta(t) \rangle = 0$  and  $\langle \eta(t) \eta(t') \rangle = \delta(t - t')$ ,  $v_0$  is the constant speed of the particle and  $D_r$  is the rotational diffusion constant.

Another one is run and tumble (RTP) [40] moving on the two-dimensional  $x - y$  plane.

$$\dot{\mathbf{r}}(t) = v_0 \boldsymbol{\sigma}(t) \quad (6)$$

where again  $v_0$  is the constant speed of the particle and  $\boldsymbol{\sigma}(t)$  is the coloured noise. It is unit vector that reorients at some constant rate  $\gamma$  to a new orientation that is randomly chosen uniformly from the unit circle. Both of these models converge to Brownian motion in appropriate limits. For instance, for the RTP, in the limit  $\gamma \rightarrow \infty$  and  $v_0 \rightarrow \infty$ , keeping the ratio  $\frac{v_0^2}{2\gamma} = D_{\text{eff}}$  fixed (where  $D_{\text{eff}}$  is the effective diffusion coefficient),  $\boldsymbol{\sigma}(t)$  becomes white noise and the typical fluctuations of the active models reduce to Brownian motion with diffusion coefficient  $D = D_{\text{eff}}$  [41].

The rest of the paper is organized as follows. Our results are all concentrated in Sec. II. We begin in subsection II A by calculating the right and left tails for the area and perimeter distributions for a single planar Brownian motion. We extend these results to  $N$  non-interacting Brownian motions in subsection II B. In subsection II C, we extend the results to active particles in  $d = 2$ , uncovering a remarkable sequence of dynamical phase transitions for the case of multiple RTPs. In subsection II D we consider higher dimensions, focusing on the volume and surface area distributions for a single Brownian particle in  $d = 3$ . We conclude with a discussion in Sec. III. Several technical details are given in the Appendices.

## II. RESULTS

The simplest case is the single Brownian particle in  $d = 2$ . We therefore begin with a full analysis of the two tails for this case, followed by extensions to multiple and/or active particles. Then we treat the case of a single Brownian particle in  $d = 3$ . The results are summarized in the table I.

Dimensions	Types of walk	Observables	Tails	Open, Closed
d=2	BM	Perimeter	right	Open: $\mathcal{P}(L) \sim e^{-L^2/16DT}$ ; Closed: $\mathcal{P}(L) \sim e^{-L^2/4DT}$
			left	$\mathcal{P}(L) \sim e^{-4\pi^2 x_1^2 DT/L^2}$ ;
		Area	right	Open: $\mathcal{P}(A) \sim e^{-\pi A/2DT}$ ; Closed: $\mathcal{P}(A) \sim e^{-\pi A/DT}$
			left	$\mathcal{P}(A) \sim e^{-\pi x_1^2 DT/A}$ ;
	$N \geq 3$ BMs	Perimeter	right	$\mathcal{P}(L) \sim e^{-b_N L^2/DT}$ , $b_N = 1/36$ .
			left	$\mathcal{P}(L) \sim e^{-4N\pi^2 x_1^2 DT/L^2}$ ;
		Area	right	$\mathcal{P}(A) \sim e^{-c_N A/DT}$ , $c_3 = 1/\sqrt{3}$ , $c_{N \geq 4} = 1/2$ .
			left	$\mathcal{P}(A) \sim e^{-N\pi^2 x_1^2 DT/A}$ ;
	Active particles	Perimeter	right	$\mathcal{P}(L) \sim e^{-T\Phi(L/2T)}$
		Area	right	$\mathcal{P}(A) \sim e^{-T\Phi(\sqrt{2\pi A/T})}$
$d > 2$	BM	Surface area	right	$\mathcal{P}(\mathcal{A}) \sim e^{-l_{\mathcal{A},d} \mathcal{A}^{2/(d-1)}/DT}$ ; $l_{\mathcal{A},3} = \pi/4$
			left	$\mathcal{P}(\mathcal{A}) \sim e^{-\tilde{f}_d DT (\tilde{\mathcal{A}}_d/\mathcal{A})^{2/(d-1)}}$
		Volume	right	$\mathcal{P}(V) \sim e^{-l_{V,d} V^{2/d}/DT}$ ; $l_{V,3} \simeq 5.3$
			left	$\mathcal{P}(V) \sim e^{-\tilde{f}_d DT (\tilde{V}_d/V)^{2/d}}$

TABLE I: Behaviors of the left and right tails of the distributions of the area and perimeter of the convex hull for different planar random walks: Brownian motion (BM), multiple Brownian motions, active particles and multiple active particles, and their extensions to  $d > 2$  dimensions. Here  $x_1 = 2.4048\dots$  is the first zero of the Bessel's function  $J_0(x)$ . The case  $N = 2$  is very simply related to the case  $N = 1$  and the relation is given by Eq. (17).  $\Phi(\mathbf{z})$  is the rate function that describes the distribution of the position of the active particle at long times, see Eq. (28). For the RTP,  $\Phi(\mathbf{z})$  is given in Eq. (29). The  $\alpha_M$  and  $\beta_M$  are the coefficients of the rate function  $\Phi(\mathbf{z})$  for the  $N \geq 3$  active particles given by Eq. (41).  $\tilde{f}_d$  is the smallest eigenvalue of the minus Laplace operator on the  $d$ -dimensional ball of unit radius with absorbing boundary conditions, and  $\tilde{V}_d$  and  $\tilde{\mathcal{A}}_d$  are the volume and surface area, respectively, of the ball of unit radius. Trajectories are open unless stated otherwise.

### A. Single planar Brownian motion

#### 1. Right tail: Large area ( $A$ ) / large perimeter ( $L$ )

Let us begin from the simplest case of a single Brownian particle. From the scaling forms (2) and (3) one immediately finds that large perimeters or areas are mathematically equivalent to the short-time and/or weak-noise limit, i.e  $DT \ll A$  or  $DT \ll L^2$ . The probability is dominated by the most probable path constrained on a given value of the observable of interest ( $A$  or  $L$ ) in a short  $T$  limit. In this short  $T$  / weak noise limit, the optimal fluctuations method (OFM) [42–53] gives the equation of the optimal path of the motion constrained to a given value of the observable of interest. The path probability of the trajectory  $\mathbf{r}(t)$  is given by

$$\mathcal{P}(\mathbf{r}(t)) \sim e^{-s/2D} \quad (7)$$

where  $s[\mathbf{r}(t)]$  is the Wiener action [1]

$$s[\mathbf{r}(t)] = \frac{1}{2} \int_0^T \dot{\mathbf{r}}(t)^2 dt. \quad (8)$$

In the small- $DT$  limit, we apply the saddle-point approximation and thus find that the dominant contribution to  $\mathcal{P}(A)$  ( $\mathcal{P}(L)$ ) comes from the minimizer  $\mathbf{r}(t)$  (the "optimal trajectory") of the action constrained on the value of the area (perimeter). The action is minimized by motion with constant speed  $|\dot{\mathbf{r}}(t)| = \text{constant}$  with the additional constraints [52–54] (see also Appendix A). The action of the optimal trajectory is thus given by

$$-\ln \mathcal{P} \simeq s = \frac{\mathcal{L}^2}{4DT} \quad (9)$$

where  $\mathcal{L}$  is the length of the trajectory. The problem thus reduces to minimizing  $\mathcal{L}$  constrained on a given value of the observable (area or perimeter).

Let us start by studying the closed case which is a little simpler. Without loss of generality we consider only trajectories that are themselves the boundary of a convex shape, because if this is not the case, one can always find a shorter trajectory with the same convex hull, see Fig. 1. Under this assumption  $\mathcal{L}$  equals the perimeter  $L$  of the convex hull.

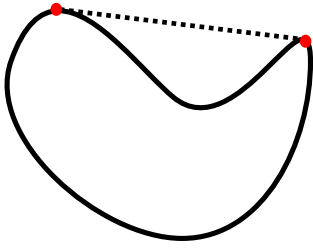


FIG. 1: Schematic diagram of the convex hull of a trajectory of a Brownian particle. To minimize the length of the trajectory  $\mathcal{L}$  constrained on the convex hull area  $A$  or perimeter  $L$ , it is more favorable to follow the dotted (straight) line than the solid line, when going between the two points marked in the figure.

Consider first the problem of minimizing  $\mathcal{L}$  constrained on  $A$ . By the argument above, the problem reduces to that of finding a shape of minimal perimeter that encloses a given area – the isoperimetric problem – whose solution has been known for a very long time [55, 56]: It is a circle of area  $A$  (see Fig. 2 (a)). The area and perimeter of a circle are related via  $A = L^2/(4\pi)$ . Hence the probability of the right tail behaves as [recalling that  $\mathcal{L} = L$  and using Eq. (9)]

$$-\ln \mathcal{P}(A \gg DT) = s = \pi \frac{A}{DT}. \quad (10)$$

Let us now find the minimizer of  $\mathcal{L}$  constrained on  $A$  for an open Brownian motion. We assume that the particle begins at the origin (at time  $t = 0$ ) and without loss of generality, that it finishes on the  $x$  axis at time  $t = T$ . We additionally assume that the trajectory is contained in the upper-half plane  $y \geq 0$  (this assumption will be justified a posteriori). As for the closed case, the minimizer cannot have any concave sections. The problem thus reduces to finding the curve of minimal length with the area under the curve constrained to a given value  $A$ . This problem is known as Dido's problem [55, 56], which is the extension of the isoperimetric problem. The solution to Dido's problem is a semi-circle of area  $A$  (see Fig. 2 (b)). For the semi-circle, the length of the trajectory and the area are related via  $A = \mathcal{L}^2/2\pi$ . Hence, the probability of the right tail for an open Brownian motion is given by

$$-\ln \mathcal{P}(A \gg DT) = s = \frac{\pi}{2} \frac{A}{DT}. \quad (11)$$

This optimal trajectory is in agreement with rigorous results from the mathematical literature which were obtained for general open random walks [37]. The result (11) is also in excellent agreement with the numerical data of Ref. [22], see Fig. 3 (a).

Now let us solve the minimization problem of the length  $\mathcal{L}$  constrained on the perimeter  $L$ . For the closed case, as shown above,  $L = \mathcal{L}$  and therefore the minimization problem has a very large degeneracy of solutions

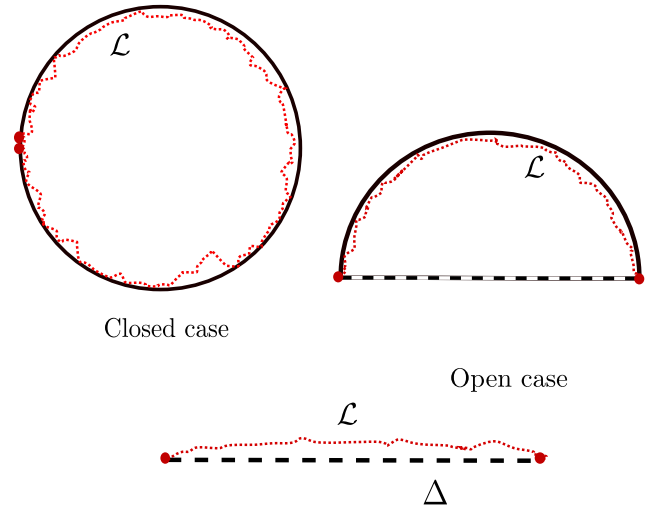


FIG. 2: Solid lines: Trajectories of minimal length  $\mathcal{L}$ , corresponding to the right tails of the area and perimeter distributions. For the area distribution, both the open and closed Brownian motions are plotted. Schematic diagrams of the convex hulls formed by Brownian particles of length  $\mathcal{L}$ , corresponding to the right tails of the area and perimeter distributions. The dotted lines are a schematic of realistic realizations that attain large, but finite area (or perimeter). For the closed case, the hull is a circle for a fixed area  $A$  and for open case, the hull is a half circle for a fixed  $A$  and line segment for fixed  $L$ .

(any closed trajectory which is the boundary of a convex shape is a minimizer). For open motion, we assume again that the trajectory stays in the upper-half plane (taking the endpoint to be on the  $x$  axis) and hence the relation between  $L$  and  $\mathcal{L}$  is  $L = \mathcal{L} + \Delta$ , where  $\Delta$  is the distance between the endpoints of the Brownian particle. The minimal  $\mathcal{L}$  is obtained when the curve approaches straight line (see Fig. 2 (c)), and then one has  $\Delta \simeq \mathcal{L}$  so

$$L = \mathcal{L} + \Delta \simeq 2\mathcal{L} \quad (12)$$

Hence, the right tail of  $\mathcal{P}(L)$  behaves as

$$-\ln \mathcal{P}(L \gg \sqrt{DT}) \sim \begin{cases} \frac{L^2}{16DT}, & \text{Open,} \\ \frac{L^2}{4DT}, & \text{Closed.} \end{cases} \quad (13)$$

The results are in excellent agreement with the numerical data of Ref. [22], see Fig. 3 (b).

## 2. Left tail: Small area ( $A$ )/ small perimeter ( $L$ )

The small  $A$  (or small  $L$ ) limit with constant  $T$  is mathematically equivalent, according to Eq. (3), to the long- $T$  limit at constant  $A$  (or constant  $L$ ). In other words, the particle must survive inside the convex hull itself for an unusually long time. The least unlikely way for this to

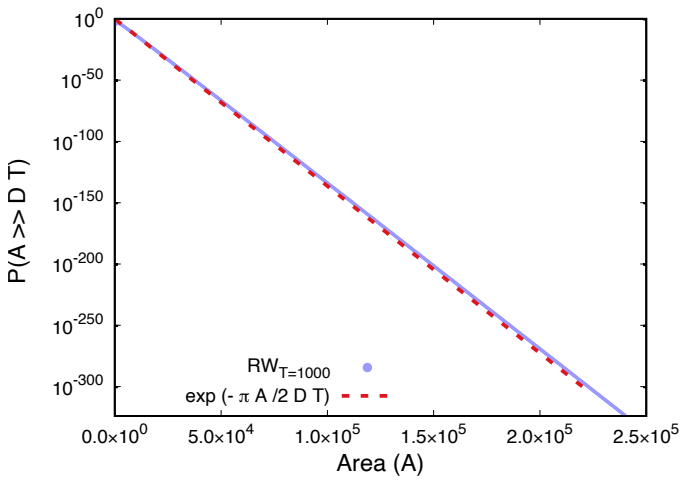
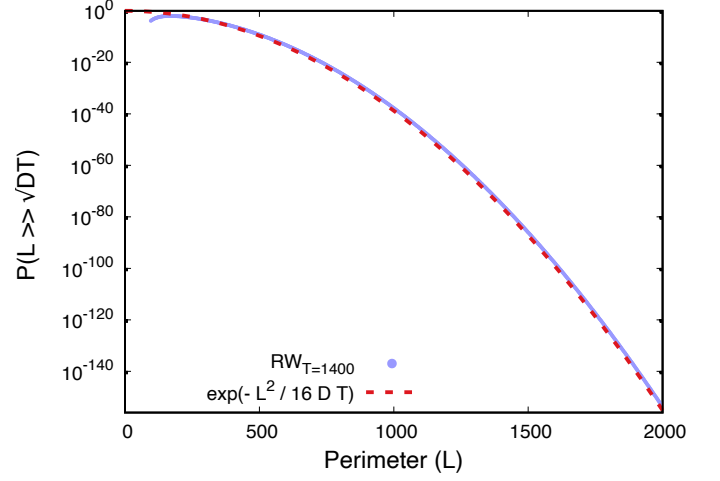
(a) Area: right tail  $A \gg DT$ , open motion(b) Perimeter: right tail  $L \gg \sqrt{DT}$ , open motion

FIG. 3: Right tails of the distributions (in log scale) of the area (a) and perimeter (b) of the convex hull for an open planar Brownian motion. The blue circles depict the data of  $\mathcal{P}(A)$  from [22] and can be seen to be in excellent agreement with the red dashed lines which denote our theoretical predictions. Parameters are  $D = 1/2$ , and  $T = 1000$  (a) and  $T = 1400$  (b).

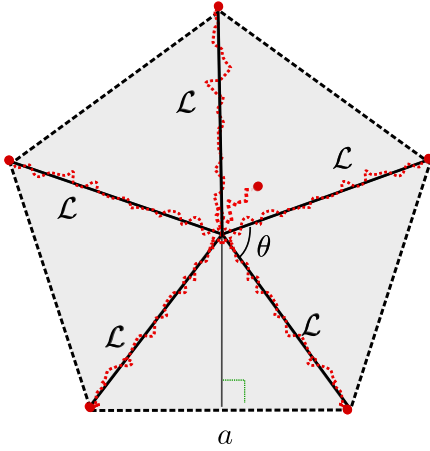


FIG. 4: Schematic diagram of the convex hull formed by  $N$  Brownian particles of length  $\mathcal{L}$ . Here  $N = 6$ ,  $M = 5$ ,  $\theta = \frac{2\pi}{M}$  is the angle between two Brownian particles participating in the solution. As explained in the text, the solutions with  $M = 3$  and  $M = 4$  are the optimal solution for perimeter and area respectively.

happen is if the convex hull takes the shape of a circle of area  $A$  (or perimeter  $L$ ). We thus argue that  $\mathcal{P}(A)$  (or  $\mathcal{P}(L)$ ) is, in the leading order, given by the survival probability inside a circle of area  $A$  (or perimeter  $L$ ). In the leading order, it does not matter whether the Brownian motion is open or closed (the difference only affects a short time window in the trajectory, close to  $t = T$ ).

In the long time limit (large  $T$ ), the survival probability  $S_{prob}(T|R)$  of a Brownian particle inside a  $d$ -dimensional ball of radius  $R$  is, in the leading order, in-

dependent of the initial position within the ball, and is dominated by the smallest eigenvalue (in absolute value) of the Laplace operator with absorbing boundary conditions. Therefore, it is given by (see e.g. [57])

$$-\ln S_{prob}(T|R) \simeq \begin{cases} \frac{\pi^2}{4R^2} DT, & d = 1, \\ \frac{x_1^2}{R^2} DT, & d = 2, \\ \frac{\pi^2}{R^2} DT, & d = 3 \end{cases} \quad (14)$$

where  $x_1 = 2.4048\dots$  is the first positive root of the Bessel function  $J_0(z)$ .

Using this, we obtain the left tails for the area and perimeter distributions by considering the survival probabilities in a circle of given area (or of given perimeter), yielding

$$-\ln \mathcal{P}(A \ll DT) \simeq \pi x_1^2 \frac{DT}{A}, \quad (15)$$

$$-\ln \mathcal{P}(L \ll \sqrt{DT}) \simeq 4\pi^2 x_1^2 \frac{DT}{L^2}. \quad (16)$$

These formulas hold both for the open and closed Brownian motions. The scaling behaviors in these results are in agreement with the numerical results in [22] but the numerical coefficients observed there were different. We believe that this discrepancy is because the numerical simulations use a sufficient number of time steps to observe the continuous Brownian motion behavior.

## B. Multiple Brownian motions

In this subsection, we consider  $N > 1$  non-interacting Brownian particles, beginning from the case  $N = 2$  which



is particularly simple. In this case, by concatenating the two trajectories we obtain a trajectory that could be considered as that of a single Brownian particle of twice the duration. Therefore, the distributions for  $N = 2$  are exactly related to those for  $N = 1$  via

$$\mathcal{P}(*, T) |_{N=2} = \mathcal{P}(*, 2T) |_{N=1} \quad (17)$$

(where the time dependence is denoted explicitly, and  $*$  represents area, perimeter or other such observables). In particular, the distribution tails can thus be obtained immediately from the results reported above for the  $N = 1$  case.

Therefore, in the rest of this subsection we will assume that  $N \geq 3$ . Let us consider first the right tail. Here, following a similar approach to the one we used above for the case  $N = 1$ , we find that this tail is dominated by the (multi-particle) trajectory that minimizes the sum of the Wiener actions  $s_{\text{tot}}$ , constrained on a given value of the area or perimeter. The minimum is obtained for trajectories for which each particle's speed is constant, and the sum of the Wiener actions is given by  $s_{\text{tot}} = (\sum_{i=1}^N \mathcal{L}_i^2) / 4DT$  where  $\mathcal{L}_i$  is the length of the trajectory of particle  $i$ .

In order to proceed to solve this minimization problem we next assume that the full trajectories of the  $N$  particles, except perhaps some of the endpoints, are all in the interior of the convex hull (this assumption will be justified a posteriori). Thus only the endpoints of these trajectories are important, and the optimal trajectories must be straight lines. This simplifies the minimization problem considerably, because now we are just minimizing a function of the endpoints (and not a functional of the entire trajectories).

For any  $3 \leq M \leq N$  there exists a solution to this minimization problem for which  $M$  of the particles travel the same distance  $\mathcal{L}_i = \mathcal{L}$  in straight lines, and leaving the origin at equally-spaced angles, while the remaining  $N - M$  particles remain near the origin. Thus, the convex hull that is formed by these trajectories is a regular polygon of  $M$  sides (see Fig. 4 for an example with  $N = 6$  and  $M = 5$  in shaded region). The action  $s_M = s_{\text{tot}}$  for each of these solutions can be expressed as

$$s_M(L) = \tilde{b}_M \frac{L^2}{DT}, \quad (18)$$

$$s_M(A) = \tilde{c}_M \frac{A}{DT}. \quad (19)$$

The coefficients  $\tilde{b}_M$  and  $\tilde{c}_M$  are of geometric origin: They are calculated from the relation between  $\mathcal{L}$  and  $L$  or  $A$  respectively for a regular  $M$ -sided polygon. For a  $M$  sided polygon (for example Fig. 4 for  $M = 5$ ), the perimeter is  $L = Ma$  where  $a = 2\mathcal{L} \sin \theta$  is the length of each side of the polygon, which implies  $L = (2M \sin \frac{\pi}{M}) \mathcal{L}$ . Similarly, the area is given by  $A = (M \sin \frac{\pi}{M} \cos \frac{\pi}{M}) \mathcal{L}^2$ . Finally, using that the total action is  $s_M = M\mathcal{L}^2 / 4DT$ , we obtain

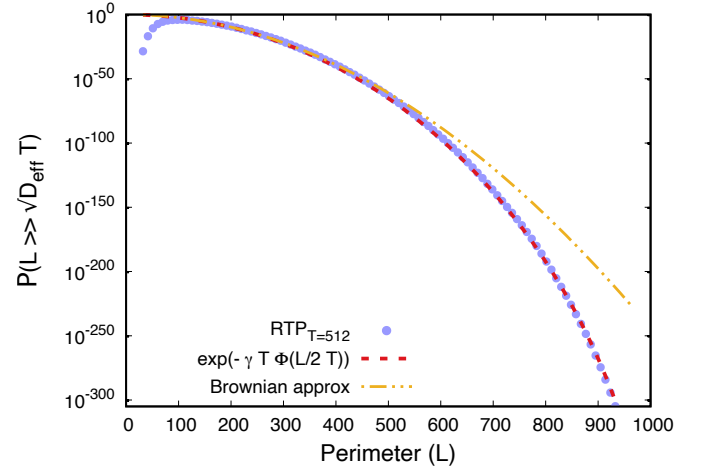


FIG. 5: Right tail of the distribution  $\mathcal{P}(L)$  of perimeter  $L$  of the convex hull for a run and tumble motion for walk length  $T = 512$  and  $\gamma = v_0 = 1$ . The blue circles depict the numerical data from [27] and the red dashed lines denote our theoretical prediction. The yellow dot-dashed line denotes the corresponding Brownian motion result, obtained by applying the parabolic Brownian approximation (36) of the rate function  $\Phi(z)$ . The Brownian approximation can be seen to correctly describe the near tail of the distribution, but it breaks down in the far tail.

the coefficients

$$\tilde{b}_M = \frac{1}{16M \sin^2 \frac{\pi}{M}}, \quad \tilde{c}_M = \frac{1}{2 \sin \frac{2\pi}{M}}. \quad (20)$$

These solutions all represent *local* minima of the action  $s_M$ , and in order to find the *global* minimum, we must now perform an additional minimization over  $M = 3, 4, \dots, N$ . This amounts to minimizing the coefficients  $\tilde{b}_M$  and  $\tilde{c}_M$  over  $M$  for the perimeter and area, respectively. These coefficients are tabulated in Table II. We find, and show explicitly in Appendix B.1, that  $M = 3$  ( $M = 4$ ) is minimal (over all values  $M = 3, 4, \dots$ ) for the perimeter (area) case. Therefore the optimal convex hull shape is an equilateral triangle whose center is the origin for the perimeter case and for the area case with  $N = 3$ , and a square centered at the origin for the area case with  $N \geq 4$ . So the probability is now expressed for any  $N \geq 3$  as (see Table I)

$$\mathcal{P}(L) \sim e^{-b_N L^2 / DT}, \quad b_N = \min_{3 \leq M \leq N} \tilde{b}_M = \tilde{b}_3 = \frac{1}{36} \quad (21)$$

$$\mathcal{P}(A) \sim e^{-c_N A / DT},$$

$$c_N = \min_{3 \leq M \leq N} \tilde{c}_M = \begin{cases} \tilde{c}_3 = \frac{1}{\sqrt{3}}, & N = 3, \\ \tilde{c}_4 = \frac{1}{2}, & N \geq 4. \end{cases} \quad (22)$$

Thus, rather remarkably, the right tail of the perimeter (area) distribution becomes, in the leading order, independent of  $N$  for  $N \geq 3$  ( $N \geq 4$ ). These theoretical

$M$	$\tilde{b}_M = (16M \sin^2 \frac{\pi}{M})^{-1}$	$\tilde{c}_M = (2 \sin \frac{2\pi}{M})^{-1}$
3	$1/36 = 0.027 \dots$	$1/\sqrt{3} = 0.57 \dots$
4	$1/32 = 0.031 \dots$	$1/2 = 0.5$
5	$(5 + \sqrt{5})/200 = 0.036 \dots$	$\sqrt{2/\sqrt{5} + 5} = 0.525 \dots$
6	$1/24 = 0.041 \dots$	$1/\sqrt{3} = 0.577 \dots$
7	$0.047 \dots$	$0.639 \dots$
$M \gg 1$	$\simeq M/16\pi^2$	$\simeq M^2/4\pi$

TABLE II: Coefficients of the action  $s_M(L)$  and  $s_M(A)$  respectively given in Eq. (18) for  $N$  non-interacting Brownian particles. the minimum is obtained at  $M = 3$  ( $M = 4$ ) for the perimeter (area) case.

predictions exhibit excellent agreement with the numerical observations from Ref. [23], see Appendix B.2.

The left tails of the distributions of  $A$  and  $L$  for  $N$  non-interacting particles behave very similarly to the single particle case. They are dominated by the survival probability of  $N$  particles inside a circle of appropriate area (or perimeter). Since the particles are noninteracting, the latter probability is simply given by that of a single particle, raised to the power  $N$ . Using the middle line of (14) together with the relations between the radius of a circle and its perimeter and area, one finds

$$\mathcal{P}(A) \sim e^{-\pi x_1^2 NDT/A}, \quad (23)$$

$$\mathcal{P}(L) \sim e^{-4\pi^2 x_1^2 NDT/L^2}. \quad (24)$$

### C. Active particles

As described above, for a broad class of models of active models, the long-time typical behavior is diffusive, with an effective diffusion coefficient that can be found (see examples above for the cases of the RTP and ABP). Thus, we expect that both the typical fluctuations and the near tails of the area and perimeter distributions behave, at long times  $T \gg \tau$  (where, to remind the reader,  $\tau$  is the correlation time of the active noise), coincide with those of Brownian motion. The signatures of activity are expected to be found in the far tails of the distribution. In this subsection, we will focus on the behavior in the right tail. The left tail probabilities are still expected to be given by the long-time survival probabilities inside circles of appropriate sizes. We do not attempt to calculate these survival probabilities in the current work, see however the recent Ref. [58] in which this was achieved for the ABP (see also the related work [59] where the RTP in  $d = 1$  was studied).

#### 1. Coarse graining

For active particles, in the long time limit (where  $T$  is much larger than the correlation time  $\tau$  of the noise  $\Sigma$ ), one can coarse grain the noise  $\Sigma(t)$  that is coarse grained by averaging it over intermediate timescales  $\tau \ll \Delta t \ll T$  [60–67].

$$\bar{\Sigma}(t) = \frac{1}{\Delta t} \int_t^{t+\Delta t} \Sigma(t') dt'. \quad (25)$$

The probability of a coarse-grained noise history  $\bar{\Sigma}(t)$  is given (in the leading order) by

$$\mathcal{P}[\bar{\Sigma}(t)] \sim \exp(-s[\bar{\Sigma}(t)]) \quad (26)$$

where the action  $s[\bar{\Sigma}(t)]$  is now given by

$$s[\bar{\Sigma}(t)] = \int_0^T \Phi[\bar{\Sigma}(t)] dt. \quad (27)$$

Here we assume that the long-time position distribution  $\mathcal{P}(x, y, t)$  of the particle satisfies an LDP with a rate function  $\Phi(z)$ , i.e., that

$$\mathcal{P}(x, y, t) \sim e^{-t\Phi(x/t, y/t)}. \quad (28)$$

$\Phi(z)$  is known for several standard models of active particles including RTP, ABP. For the RTP (Eq. 6) it was calculated exactly to be [41, 67, 68]

$$\Phi(v) = 2\gamma\phi(v/v_0), \quad \phi(z) = 1 - \sqrt{1 - z^2}. \quad (29)$$

For ABP (see Eq. 5), the  $\Phi$  was found exactly in [69–71] in terms of the smallest eigenvalue that gives periodic solutions to the Mathieu equation.

The coarse-grained Langevin equation, obtained by replacing  $\Sigma(t)$  by  $\bar{\Sigma}$  in Eq. (4) is

$$\dot{r}(t) = \bar{\Sigma}(t). \quad (30)$$

For rotationally invariant statistics of the noise  $\Sigma(t)$ , the  $\Phi[z]$  is also rotationally symmetric  $\Phi[z] = \Phi[z]$ .

As in the case of Brownian motion, the minimizer of (27) is obtained for trajectories for which the argument of  $\Phi$  is of constant modulus which simply equals the speed  $\mathcal{L}/T$  (see Appendix A). Therefore, we simply get

$$s = T\Phi(\mathcal{L}/T) \quad (31)$$

where  $\mathcal{L}$  is the length of the trajectory. Thus, we find that here too, the problem boils down to minimizing  $\mathcal{L}$  under the constraints.

#### 2. Right tail for a single active particle

Using Eq. (31), we find that the right tails of the area and perimeter distributions can be calculated by replacing  $\mathcal{L}^2/4DT$  in Eq. (9) by  $T\Phi(\mathcal{L}/T)$ . Thus, the right tails

of the perimeter and area distributions for the closed and open cases are given by:

$$\ln \mathcal{P}(L) \simeq \begin{cases} -\gamma T \Phi(L/T), & \text{Closed,} \\ -\gamma T \Phi(L/2T), & \text{Open,} \end{cases} \quad (32)$$

$$\ln \mathcal{P}(A) \simeq \begin{cases} -\gamma T \Phi(\sqrt{4\pi A}/T), & \text{Closed,} \\ -\gamma T \Phi(\sqrt{\pi A}/T), & \text{Open.} \end{cases} \quad (33)$$

To give an explicit, concrete example, let us consider the RTP. For the RTP, using Eq. (29) the right distribution tails for the open case are given by

$$\ln \mathcal{P}(L) \simeq -\gamma \left( T - \sqrt{T^2 - \frac{L^2}{v_0^2}} \right); \quad L \gg \sqrt{D_{\text{eff}} T} \quad (34)$$

$$\ln \mathcal{P}(A) \simeq -\gamma \left( T - \sqrt{T^2 - \frac{4\pi A}{v_0^2}} \right); \quad A \gg D_{\text{eff}} T \quad (35)$$

where  $D_{\text{eff}}$  is the effective diffusion coefficient. Fig. 5 shows the right tail of the perimeter for  $T = 512$ , which fits well with the experimental data from [27]. For small  $|z| \ll 1$ , the  $\Phi(z)$  can be approximated as a parabola

$$\Phi(z) \simeq \frac{z^2}{2} \quad (36)$$

which corresponds to passive limit and the action in Eq. (27) reduces to the Wiener action (8) [1], which is the Brownian motion limit. As a result, the near right tail of the distribution,  $\sqrt{D_{\text{eff}} T} \ll L \ll v_0 T$ , coincides with that of the Brownian motion result, see Fig. 5.

### 3. Dynamical phase transitions for multiple active particles

Let us now analyze the case of  $N > 1$  active particles. We first consider the case  $N = 2$ . At  $T \gg \tau$ , the argument used above for Brownian particles, to relate the cases  $N = 2$  and  $N = 1$ , still holds (but only approximately). Thus, Eq. (17) still approximately holds at long times, both in the typical-fluctuations and large-deviation regimes.

Let us now analyze the case  $N \geq 3$ , focusing on the right tail. The analysis is similar to the case of  $N \geq 3$  Brownian particles studied above (see Sec. II B). One must minimize the sum of the coarse-grained actions  $s_{\text{tot}} = T \sum_{i=1}^N \Phi(\mathcal{L}_i/T)$ . We again assume that the trajectories of the  $N$  active particles reside within the interior of the convex hull, except for some of the trajectories' endpoints. Thus, the optimal paths are all straight lines, and the problem reduces to that of minimizing  $s_{\text{tot}}$  with respect to the endpoints of the trajectories. Again we find that for each  $3 \leq M \leq N$  there exists a solution in which  $M$  particles exit the origin at equally-spaced angles, and each travel a distance of  $\mathcal{L}_i = \mathcal{L}$ , while the remaining  $N - M$  particles stay near the origin, creating

a convex hull whose shape is a regular polygon with  $M$  sides, see Fig. 4. However, the actions  $s_M = s_{\text{tot}}$  of these solutions,  $s_M = M T \Phi(\mathcal{L}/T)$ , are different to those of the Brownian particles' case. As a result, the optimal value of  $M$  may too be different, and as we show below, it can in fact change within the tail, leading to dynamical phase transitions which are generically of the first order.

Therefore, the right tails of the perimeter and area distributions are determined by the solution with optimal  $M$ , i.e. that minimizes  $s_M$ ,

$$\mathcal{P}(L) \sim e^{-T \Psi_N(L/T)}, \quad (37)$$

$$\mathcal{P}(A) \sim e^{-T \Psi_N(\sqrt{A}/T)}, \quad (38)$$

where the large-deviation functions  $\Psi_N$  are related to the  $s_M$ 's above via

$$\Psi_N(L/T) = \min_{3 \leq M \leq N} M \Phi(\alpha_M L/T), \quad (39)$$

$$\Psi_N(\sqrt{A}/T) = \min_{3 \leq M \leq N} M \Phi(\beta_M \sqrt{A}/T). \quad (40)$$

Here the coefficients  $\alpha_M$  and  $\beta_M$  are calculated from the geometric relation between  $\mathcal{L}$  and  $L$  or  $A$  respectively similar like the multiple Brownian motions in Fig. 4 in Sec. II B, i.e.  $L = (2M \sin \frac{\pi}{M}) \mathcal{L}$  and  $A = (M \sin \frac{\pi}{M} \cos \frac{\pi}{M}) \mathcal{L}^2$ . Hence the  $\alpha_M$  and  $\beta_M$  are related to  $\tilde{b}_M$  and  $\tilde{c}_M$  as:

$$\alpha_M = 4\sqrt{M \tilde{b}_M} = \frac{1}{2M \sin \frac{\pi}{M}}, \quad (41)$$

$$\beta_M = 2\sqrt{\tilde{c}_M/M} = \frac{1}{\sqrt{M \sin \frac{\pi}{M} \cos \frac{\pi}{M}}}. \quad (42)$$

Let us now give explicit results for the particular case of multiple RTPs. Here the rate functions are conveniently written as

$$\Psi_N(v) = 2\gamma \psi_N(v/v_0) \quad (43)$$

where the  $\psi_N$ 's are dimensionless, and are given by

$$\psi_N(z) = \min_{3 \leq M \leq N} \tilde{\psi}_M(z) \quad (44)$$

and  $\tilde{\psi}_M$  is related to the dimensionless rate function  $\phi$  in Eq. (29) that describes the position distribution of a single particle,

$$\begin{aligned} \tilde{\psi}_M(z) &= M \phi(a_M z) = M \left( 1 - \sqrt{1 - a_M^2 z^2} \right) \\ &= \begin{cases} M \left[ 1 - \sqrt{1 - \frac{z^2}{4M^2 \sin^2(\pi/M)}} \right] & \text{(perimeter)} \\ M \left[ 1 - \sqrt{1 - \frac{z^2}{M \sin(\pi/M) \cos(\pi/M)}} \right] & \text{(area)} \end{cases} \end{aligned} \quad (45)$$

where  $a_M = \alpha_M, \beta_M$  for perimeter and area respectively.

In the near right tails, the value of  $M$  that dominates is the same as for the case of Brownian particles. For  $T \gg$



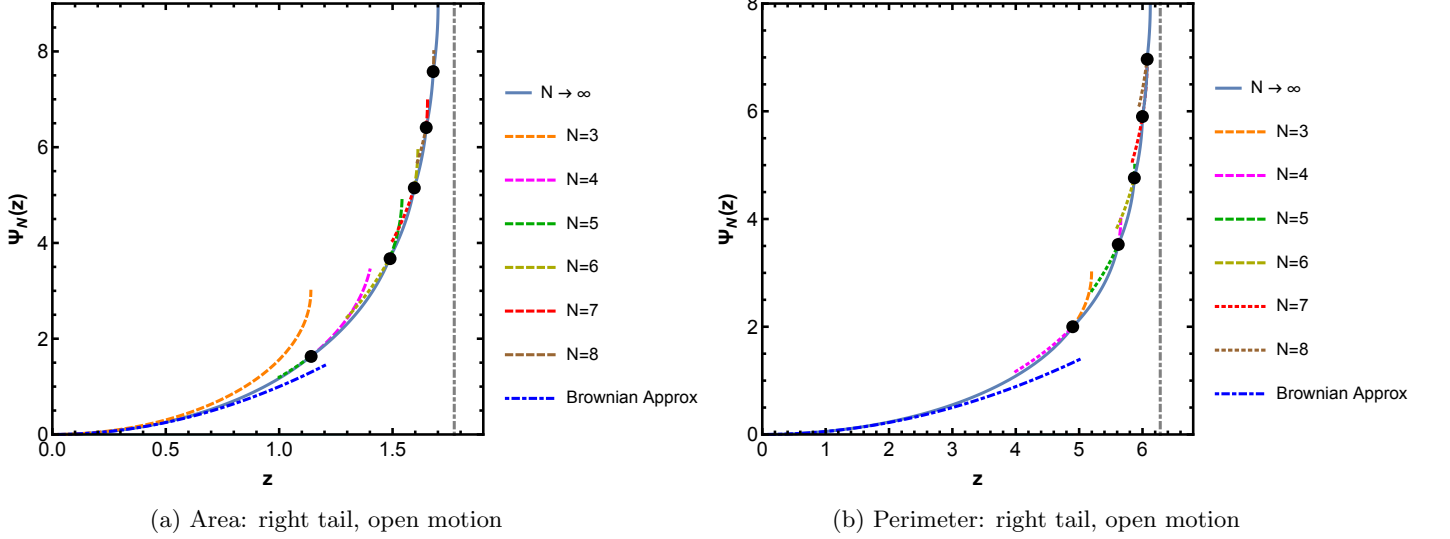


FIG. 6: The large deviation function  $\psi_N(z)$  for  $N$  RTPs that describes the right distribution tail for **(a)** Area  $A$  and **(b)** Perimeter  $L$  for  $N$  RTPs. The solid blue line depicts  $\psi_{N \rightarrow \infty}$  while the dashed lines correspond to  $\psi_N$  for finite values of  $N$ . The dotted lines correspond to  $\tilde{\psi}_M$  in regions where they are not optimal for any value of  $N$ . The circles denote the critical points  $z_M$  at which the optimal solution changes from one local minima ( $M$ ) to another local minima ( $M + 1$ ), signalling a first-order dynamical phase transition. The blue dot-dashed lines correspond to the Brownian motion approximations [for  $N \geq 4$  in (a)], and are seen to give the correct asymptotic behavior at  $z \ll 1$ , describing the near right tail of the distribution. The vertical, grey dot-dashed lines denote the value that the area or perimeter cannot possibly exceed for any  $N$ , corresponding to a convex hull which is a circle of radius  $v_0 T$ .

$\tau$ , the right tail of the  $N$  active particles behave like the  $N$  noninteracting Brownian particles where the action for  $M = 3$  in case of perimeter and  $M = 4$  in case of area dominates. Further into the right tail (for sufficiently large  $N$ ), however, activity dominates and the  $M = 4$  (for perimeter) and  $M = 5$  (for area) becomes the optimal solution. This leads to singularity in the LDF  $\psi_N(z)$  which we interpret as a dynamical phase transition, at a critical value of  $z$ , shown by the solid black circle in Fig. 6. Further into the tail further successive DPTs occur from  $M = i$  to  $M = i + 1$  for  $i = 3, \dots, M - 1$  in case of perimeter and for  $i = 4, \dots, M - 1$  in case of area. So the right tail of the distribution exhibits  $N - 3$  and  $N - 4$  DPTs for perimeter and area respectively. As the transitions occur when the graphs of two  $\tilde{\psi}_M$ 's cross each other, this transition is of first order in nature, i.e., the first derivative of  $\psi_N$  jumps at the critical point.

The coordinates of the critical points can be calculated by requiring  $\tilde{\psi}_M(z) = \tilde{\psi}_{M+1}(z)$ , which, using Eq. (45) gives

$$M \left( 1 - \sqrt{1 - a_M^2 z^2} \right) = (M + 1) \left( 1 - \sqrt{1 - a_{M+1}^2 z^2} \right). \quad (46)$$

The solution to this equation yields the critical points  $z = z_M$ , which are given by

$$z_M = - \frac{2\sqrt{M(M+1)}\sqrt{a_{M+1}^2(M+1) - a_M^2 M}}{a_M^2 M^2 - a_{M+1}^2(M+1)^2}. \quad (47)$$

The first few critical points are at

$$z_3 = 2\sqrt{6} = 4.898\dots, \quad z_4 = 2\sqrt{8\sqrt{5} - 10} = 5.617\dots \quad (48)$$

for the perimeter, and at

$$z_4 = 1.141\dots, \quad z_5 = 1.489\dots \quad (49)$$

for the area respectively. The corresponding critical values of  $L$  and  $A$  are given by  $L = z_M v_0 T$  and  $A = (z_M v_0 T)^2$ .

More generally, it is reasonable to expect that similar DPTs may occur in many models of active particle, and not just in the particular case of the RTP as shown here. In particular, if the particle's speed is bounded e.g., for the ABP we conjecture that the qualitative picture is very similar to that of the RTP.

#### D. $d > 2$

Let us now consider the convex hull in higher dimensions ( $d > 2$ ). The arguments above can be extended straightforwardly to study the volume ( $V$ ) and surface area ( $\mathcal{A}$ ) distributions of the convex hull in higher dimensions  $d > 2$ . For instance, for a single Brownian

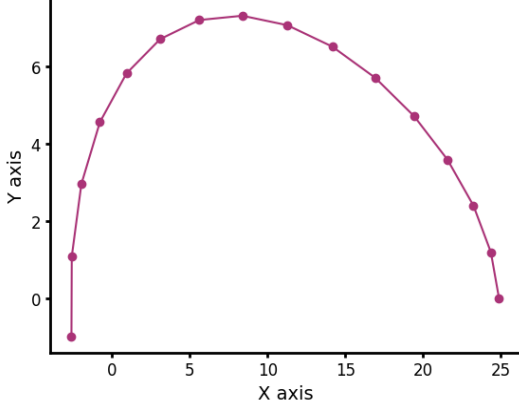


FIG. 7: The shortest curve in the three dimensional space whose convex hull has a given surface area, obtained numerically using a gradient-descent algorithm. The figure shows the projection of the trajectory onto the  $xy$  plane. The  $z$  components of all the points is negligible compared to the scale of the figure.

particle, this leads to the following behaviors in the tails:

$$\mathcal{P}(V) \sim \begin{cases} e^{-l_{V,d} V^{2/d}/DT}, & V \gg (DT)^{d/2} \\ e^{-\tilde{f}_d DT (\tilde{V}_d/V)^{2/d}}, & V \ll (DT)^{d/2} \end{cases} \quad (50)$$

$$\mathcal{P}(\mathcal{A}) \sim \begin{cases} e^{-l_{\mathcal{A},d} \mathcal{A}^{2/(d-1)}/DT}, & \mathcal{A} \gg (DT)^{(d-1)/2} \\ e^{-\tilde{f}_d DT (\tilde{\mathcal{A}}_d/\mathcal{A})^{2/(d-1)}}, & \mathcal{A} \ll (DT)^{(d-1)/2} \end{cases} \quad (51)$$

Here  $\tilde{f}_d$  is the smallest eigenvalue of the minus Laplace operator on the  $d$ -dimensional ball of unit radius with absorbing boundary conditions,  $\tilde{V}_d$  and  $\tilde{\mathcal{A}}_d$  are the volume and surface area, respectively, of the ball of unit radius (see e.g. Ref. [57]), and  $l_{V,d}$  ( $l_{\mathcal{A},d}$ ) is a coefficient calculated from the geometric relations between the  $\mathcal{L}$  and  $V$  ( $\mathcal{A}$ ) in  $d > 2$  dimensions. The coefficients for the right tails are found by minimizing  $\mathcal{L}$  constrained on  $V$  (or  $\mathcal{A}$ ). This minimization problem appears to become more difficult as  $d$  is increased. The scaling behaviors (50) were conjectured and numerically observed in Ref. [24].

For  $d = 3$  we conjecture that the curve of minimal length constrained on a convex-hull surface area  $\mathcal{A}$  is in fact confined to a plane (which, without loss of generality, can be taken to be the  $xy$  plane), and follows the edge a semi circle of area  $\mathcal{A}/2$ . The convex hull is thus a semi-circle shaped slice of infinitesimal width, so its surface area is  $\mathcal{A}$ . The reasoning behind this conjecture is as follows. The curve is optimal with respect to deformations within the  $xy$  plane – this follows from the solution to the  $d = 2$  problem conditioned on the area  $A$  (see above). On the other hand, both the curve's length  $\mathcal{L}$  and the convex hull's surface area  $\mathcal{A}$  are mirror symmetric with respect to deformations of the curve in the  $z$  direction (perpendicular to the curve). It follows that

for the semi-circular curve, the variation of  $\mathcal{L}$  constrained on  $\mathcal{A}$  indeed vanishes, and therefore this curve is a natural candidate for the (global) constrained minimizer. For this curve,  $\mathcal{A}$  and  $\mathcal{L}$  are related via  $\mathcal{A}/\mathcal{L}^2 = \pi$  and using this in Eq. (9) leads to a coefficient of  $l_{\mathcal{A},d=3} = \pi/4$ .

Very strong evidence in favor of our conjecture is that this coefficient is in agreement with the numerically-observed coefficient from Ref. [24], see [72]. To further verify our conjecture, we numerically minimized  $\mathcal{L}$  constrained on  $\mathcal{A}$  using a gradient descent algorithm, and found that the shortest curve conditioned on a given surface area indeed appears to be a semi circle (see Fig. 7). To summarize, the scaling behaviors of the tails of the surface-area distribution in  $d = 3$  are given by

$$\mathcal{P}(\mathcal{A}) \sim \begin{cases} e^{-\pi \mathcal{A}/4DT}, & \mathcal{A} \gg DT \\ e^{-4\pi^3 DT/\mathcal{A}}, & \mathcal{A} \ll DT \end{cases} \quad (52)$$

where we also plugged in the values of  $\tilde{f}_3$  and  $\tilde{\mathcal{A}}_3$ .

For the volume (in  $d = 3$ ) we were not able to obtain an analytical result for the coefficient  $l_{V,3}$ , but it was found numerically to be  $\simeq 5.3$  in Ref. [24] (see [72]). The tail behaviors of the volume distribution are thus given by

$$\mathcal{P}(V) \sim \begin{cases} e^{-5.3 V^{2/3}/DT}, & V \gg (DT)^{3/2} \\ e^{-(4\pi^2/3)^{2/3} DT/V^{2/3}}, & V \ll (DT)^{3/2} \end{cases} \quad (53)$$

where we plugged in the values of  $\tilde{f}_3$  and  $\tilde{V}_3$ .

One can extend the analysis to  $N > 1$  particles and/or to active particles, as we did above for the case  $d = 2$ , but we will not do so here. We do expect, however, that some of the qualitative features that we found in  $d = 2$  will hold in arbitrary  $d$ . In particular, we expect that: (i) The relations found above between  $N = 2$  and  $N = 1$  hold in arbitrary  $d$ . (ii) In the leading order, the right tails of  $P(V)$  and  $P(\mathcal{A})$  become independent of  $N$  for sufficiently large  $N$ . (iii) For  $N$  active particles, the right tails of  $P(V)$  and  $P(\mathcal{A})$  will be described by LDFs that are simply-related to the rate function  $\Phi$ , and for sufficiently large  $N$ , first-order DPTs will occur.

### III. DISCUSSION

We analytically studied the tails of the distributions of area  $A$  and perimeter  $L$  of convex hulls formed by the motion of active or passive particles in the plane, and analogous quantities in  $d > 2$ . We achieved this by identifying the scenario(s) that dominate the contribution to the probabilities of the rare events in question. Our findings are summarized in Table I.

In the left tails, the scenario is that of long-time survival of the particles inside a circle of appropriate size. In the right tails, the OFM is valid, i.e., the probabilities are dominated by the most likely trajectory (or coarse-grained trajectory in the case of active particles) constrained on the observable. Remarkably, we found that

the right tails of  $\mathcal{P}(L)$  and  $\mathcal{P}(A)$  for  $N$  Brownian motions become, in the leading order, independent of  $N$  at  $N \geq 3$  and  $N \geq 4$  respectively. This is because the optimal path involves significant motion of only three (four) of the particles for the perimeter (area) distribution.

For a single arbitrary rotational-invariant active particle, we calculated the exact large-deviation functions (LDFs) that describe the right tails of the distributions of the area and perimeter at times  $T$  that are much longer than the microscopic characteristic timescale of the particle. Remarkably, we found that these LDFs are simply related to the rate function  $\Phi$  that describes the long-time position distribution of the active particle, see Eqs. (32) and (33). We then extended these results to  $N$  non-interacting active particles, see Eqs. (39) and (40). We found that, depending on  $\Phi$ , there may be dynamical phase transitions (DPTs) in the right tails, signalling a sudden change in the behavior of the system as critical values of  $L$  (or  $A$ ) are crossed. We illustrated this by calculating the LDFs explicitly for the case of the RTPs, where we found that for  $N > 3$  ( $N > 4$ ), the right tail of the perimeter (area) distribution exhibits  $N - 3$  ( $N - 4$ ) such DPTs, which are all of the first order. Note that although we stated our results in the context of active particles, they are more general and cover a broad class of models (e.g. random walks that are discrete in time and/or space) for which the large-deviation principle (28) holds (with a rotationally-invariant  $\Phi$ ).

Finally, we have considered the distribution of surface area and hyper-volume of the convex hull for a Brownian motion in  $d > 2$  dimensions, with special emphasis on the case  $d = 3$ . We calculated the left tails: They are again given by the survival probability inside a hyper-sphere of appropriate size. We were able to obtain the scaling behavior in the right tails up to a numerical constant, which is found by solving a minimization problem. This problem appears to be difficult to solve analytically in general, but we were able to obtain its solution for the surface area case in  $d = 3$ . In other cases, one can solve the problem numerically.

In many of the cases that we studied here, we were able to compare our theoretical predictions with existing numerical data, showing excellent agreement in the right tails in all cases. We hope that this work will stimulate additional numerical investigations (in particular, in the left tails where we believe that more extensive numerical work is needed in order to observe convergence to the theoretical results).

Several interesting future directions of research remain. It would be interesting to extend our results to non-rotationally-invariant active particles [38]. Another interesting future direction is to analytically study the tail distributions for self-avoiding random walks, which were investigated numerically in Refs. [25, 26]. Finally, it would be interesting to study the left tails for active particles (by analyzing their long-time survival probabilities in circles of given sizes) and also to study the  $N \gg 1$  limiting behaviors of the distributions [23], both for active and

passive particles.

## Acknowledgments

We thank Baruch Meerson, Grégory Schehr and Satya Majumdar for useful discussions. We are very grateful to Hendrik Schawe, Timo Dewenter and Alexander Hartmann for sending numerical data of Refs. [22, 23, 27]. We acknowledge support from the Israel Science Foundation (ISF) through Grant No. 2651/23.

## Appendix A: Minimal-action trajectories have constant speed

In this appendix we show that the optimal paths have constant speed. We will show it for active particles with rate function  $\Phi$ , and treat Brownian motion as a particular case in which  $\Phi(z) \propto z^2$ . For concreteness, we treat the case  $d = 3$ , but the proof immediately extends to any dimension.

The action of a trajectory of an active particle in  $d = 3$ , corresponding to the coarse-grained equation (30), is

$$s[\vec{r}(t)] = \int_0^T \Phi\left(\sqrt{\dot{x}^2 + \dot{y}^2 + \dot{z}^2}\right) dt. \quad (\text{A1})$$

Consider a given curve in the  $xyz$  space, represented in parametric form by  $(x_0(s), y_0(s), z_0(s))$  with  $0 \leq s \leq 1$ . Then all time-dependent trajectories that follow this curve can be written in the form

$$(x(t), y(t), z(t)) = (x_0(f(t)), y_0(f(t)), z_0(f(t))) \quad (\text{A2})$$

for some monotonically-increasing function  $f : [0, 1] \rightarrow [0, 1]$  that satisfies  $f(0) = 0$ ,  $f(1) = 1$ .

Restricting ourselves to trajectories that follow such a curve, we rewrite the action (A1) as a functional of the function  $f$ . By using the chain rule in (A1) one obtains

$$s[\vec{r}(t)] = \int_0^T \Phi\left(\dot{f} \sqrt{x_0'^2 + y_0'^2 + z_0'^2}\right) dt \quad (\text{A3})$$

where we use the shorthand notation  $x_0' \equiv x_0'(f(t))$ , and similarly for  $y_0'$  and  $z_0'$ . The Lagrangian  $L = \Phi\left(\dot{f} \sqrt{x_0'^2 + y_0'^2 + z_0'^2}\right)$  does not explicitly depend on time  $t$ , so the Hamiltonian  $H$  is conserved. In order to calculate  $H$ , we calculate the conjugate momentum of  $f$ ,

$$p = \frac{\partial L}{\partial \dot{f}} = \Phi'\left(\dot{f} \sqrt{x_0'^2 + y_0'^2 + z_0'^2}\right) \sqrt{x_0'^2 + y_0'^2 + z_0'^2}, \quad (\text{A4})$$

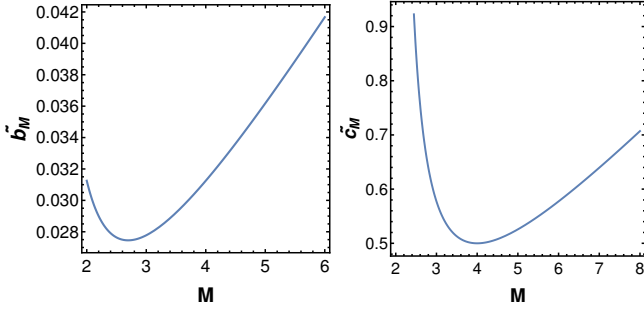


FIG. 8: Coefficients  $\tilde{b}_M$  and  $\tilde{c}_M$  as a function of  $M$ .

The  $M = 3$  and  $M = 4$  are optimal solutions for perimeter and area respectively, i.e., they minimize the functions  $\tilde{b}_M$  and  $\tilde{c}_M$  over integer values  $M \geq 3$ .

which yields

$$\begin{aligned}
 H &= \dot{f}p - L \\
 &= \dot{f} \sqrt{x_0'^2 + y_0'^2 + z_0'^2} \Phi' \left( \dot{f} \sqrt{x_0'^2 + y_0'^2 + z_0'^2} \right) \\
 &\quad - \Phi \left( \dot{f} \sqrt{x_0'^2 + y_0'^2 + z_0'^2} \right) \\
 &= E = \text{constant in time.}
 \end{aligned} \tag{A5}$$

So  $H$  is conserved in time. One can rewrite  $H$  in Eq. (A5) as a function only of the speed  $v = \sqrt{\dot{x}^2 + \dot{y}^2 + \dot{z}^2}$ , as  $H = v \Phi'(v) - \Phi(v)$ . It follows that the speed along the trajectory is constant in time, and is given by

$$\sqrt{\dot{x}^2 + \dot{y}^2 + \dot{z}^2} = \text{const} = \mathcal{L}/T \tag{A6}$$

where  $\mathcal{L}$  is the length of the curve  $(x_0, y_0, z_0)$ . Plugging this back into Eq. (A1) one finds that the action evaluated along the optimal trajectory (constrained on a given curve  $(x_0, y_0, z_0)$ ) is given by

$$s[\vec{r}(t)] = \int_0^T \Phi \left( \frac{\mathcal{L}}{T} \right) dt = T \Phi \left( \frac{\mathcal{L}}{T} \right). \tag{A7}$$

The expression (A7) is an increasing function of  $\mathcal{L}$ , and therefore, its minimization with respect to curves  $(x_0, y_0, z_0)$  (under various constraints such as convex-hull perimeter or area) boils down to the minimization of the length of the curve (under the constraints), as explained in the main text.

It is straightforward to extend this argument to arbitrary dimension  $d > 1$ .

## Appendix B: Multiple Brownian motions

### 1. Showing that $M = 3, 4$ are optimal

In this section, we explicitly show that  $M = 3$  and  $M = 4$  solutions are optimal for multiple Brownian motions for perimeter and area respectively, as stated in Sec. II B. As tabulated in Table II, the coefficients  $\tilde{b}_M$  and  $\tilde{c}_M$  of the action

$$\tilde{b}_M = \frac{1}{16M \sin^2 \frac{\pi}{M}}, \quad \tilde{c}_M = \frac{1}{2 \sin \frac{2\pi}{M}}. \tag{B1}$$

obtain their minima at  $M = 3$  and  $M = 4$  respectively.

It is fairly easy to see that  $\tilde{c}_M$  attains its minimum (for  $M \geq 2$ ) at  $M = 4$ . This is because for  $M = 4$ , the sine function in the denominator attains its maximal value 1. Let us now show that  $\tilde{b}_M$  attains its minimum (for integer  $M > 2$ ) at  $M = 3$ . For this, let us first minimize  $\tilde{b}_M$  for real values of  $M > 2$ , or equivalently, maximize  $g(M) = 1/\tilde{b}_M = 16M \sin^2 \frac{\pi}{M}$ . The requirement  $g'(M) = 0$  yields the transcendental equation

$$\tan \frac{\pi}{M} = \frac{2\pi}{M}. \tag{B2}$$

This equation has a unique (real) solution,  $M = 2.695\dots$ , which corresponds to the global minimum of  $\tilde{b}_M$  for real  $M > 2$ . Therefore, the minimum of  $\tilde{b}_M$  for integer  $M > 2$  is at  $M = 3$ .  $\tilde{b}_M$  and  $\tilde{c}_M$  are plotted, as functions of real  $M$ , in Fig. 8.

### 2. Comparison with numerics

In this subsection, we compare our expressions (21) and (22) for the right tails of the convex-hull perimeter and area distributions for  $N$  non interacting Brownian motions with the numerical data taken from [23] (see Fig. 9). We used *webplotdigital* software to collect the data from the Figs. 11 and 12 of Ref. [23]. The numerical data provided in Ref. [23] is for random walk in discrete time and standard Gaussian step distribution. The parameters that they chose were such that the time step was unity, corresponding to a diffusion coefficient  $D = 1/2$ , and they used  $T = 50$ .

For the perimeter distribution, we observe excellent agreement with our prediction for the coefficient  $b_N = \frac{1}{36}$ , for all  $N \geq 3$  (see Fig. 9a). Indeed, we find that the numerical data for  $N = 3$  and  $N = 4$  both fall on the same theoretical curve. For the area distribution, we find that the numerical results are in excellent agreement with our predictions for the coefficients,  $c_3 = 1/\sqrt{3}$  and  $c_N = 1/2$  for all  $N \geq 4$ . Indeed, we find that the numerical results for  $N = 4$  and  $N = 6$  both fall on the same theoretical curve (see Fig. 9b).

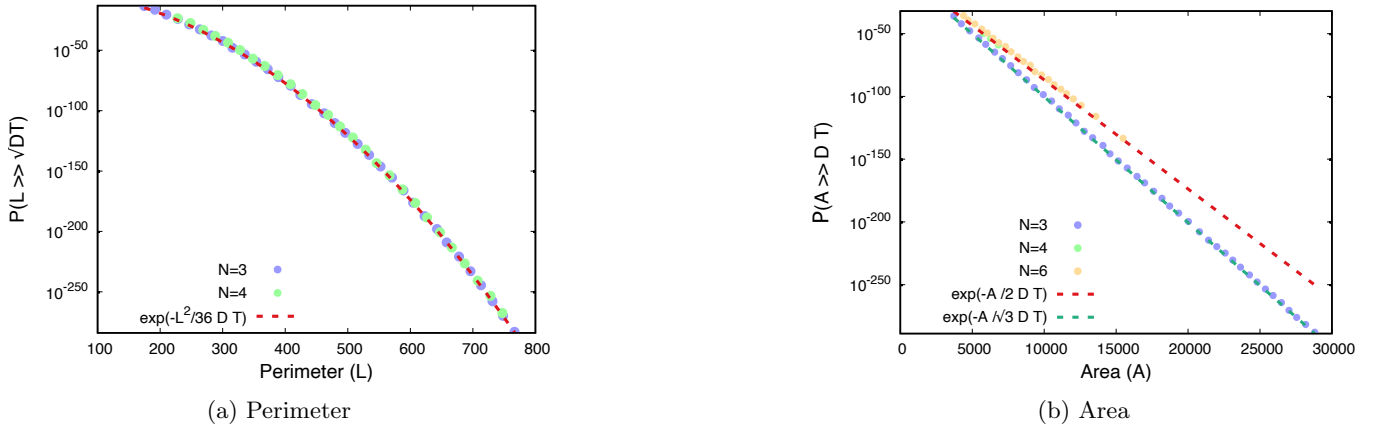


FIG. 9: Right tail distribution of **(a)**  $\mathcal{P}(L)$  and **(b)**  $\mathcal{P}(A)$  for multiple Brownian particles. The circles depict the data of the distribution from [23] and the dashed lines denote our theoretical predictions for the distribution tails.

- 
- [1] S. N. Majumdar, *Brownian Functionals in Physics and Computer Science*, *Current Science* **89**, 2076 (2005).
- [2] F. Schweitzer, *Brownian Agents and Active Particles: Collective Dynamics in the Natural and Social Sciences*, Springer: Complexity, Berlin, (2003).
- [3] P. Romanczuk, M. Bar, W. Ebeling, B. Lindner, and L. Schimansky-Geier, *Active Brownian particles*, *Eur. Phys. J. Special Topics* **202**, 1 (2012).
- [4] M. C. Marchetti, J. F. Joanny, S. Ramaswamy, T. B. Liverpool, J. Prost, M. Rao, and R. Aditi Simha, *Hydrodynamics of soft active matter*, *Rev. Mod. Phys.* **85**, 1143 (2013).
- [5] É. Fodor, M. Guo, N. Gov, P. Visco, D. Weitz, and F. van Wijland, *Activity-driven fluctuations in living cells*, *Europhys. Lett.* **110**, 48005 (2015).
- [6] O. Granek, Y. Kafri, M. Kardar, S. Ro, A. Solon, J. Tailleur, *Inclusions, Boundaries and Disorder in Scalar Active Matter*, [arXiv:2310.00079](#).
- [7] X. Trepát, M. Wasserman, T. Angelini, E. Millet, D. A. Weitz, J. P. Butler and J. J. Fredberg *Physical forces during collective cell migration*, *Nature Phys* **5**, 426–430 (2009).
- [8] H. Berg, D. A. Brown, *Chemotaxis in Escherichia coli analysed by Three-dimensional Tracking.*, *Nature* **239**, 500–504 (1972).
- [9] W. Alt, *Biased random walk models for chemotaxis and related diffusion approximations*, *J. Math. Biology* **9**, 147–177 (1980).
- [10] T. Vicsek, A. Czirók, E. Ben-Jacob, I. Cohen, and O. Shochet, *Novel Type of Phase Transition in a System of Self-Driven Particles*, *Phys. Rev. Lett.* **75**, 1226, (1995)
- [11] J. Tailleur and M. E. Cates, *Statistical Mechanics of Interacting Run-and-Tumble Bacteria*, *Phys. Rev. Lett.* **100**, 218103, (2008)
- [12] A. Dhar, A. Kundu, S. N. Majumdar, S. Sabhapandit, and G. Schehr, *Run-and-tumble particle in one-dimensional confining potentials: Steady-state, relaxation, and first-passage properties*, *Phys. Rev. E* **99**, 032132, (2019).
- [13] M. E. Cates and J. Tailleur, *Motility-Induced Phase Separation* *Annu. Rev. Condens. Matter Phys.* **6** 219, (2015).
- [14] A. B. Slowman, M. R. Evans, and R. A. Blythe, *Jamming and Attraction of Interacting Run-and-Tumble Random Walkers*, *Phys. Rev. Lett.* **116**, 218101, (2016)
- [15] B. J. Worton, *A Convex Hull-Based Estimator of Home-Range Size*, *Biometrics* **51**, 1206 (1995).
- [16] L. Giuggioli, J. R. Potts, and S. Harris, *Animal Interactions and the Emergence of Territoriality*, *PLOS Computational Biology* **7**, 1 (2011).
- [17] Y. Lanoiselée and D. S. Grebenkov, *Unraveling intermittent features in single-particle trajectories by a local convex hull method*, *Phys. Rev. E* **96**, 022144, (2017).
- [18] E. Dumonteil, S. N. Majumdar, A. Rosso, and A. Zoia, *Spatial extent of an outbreak in animal epidemics*, *Proceedings of the National Academy of Sciences* **110** 4239–4244, (2013)
- [19] G. Letac, *An Explicit Calculation of the Mean of the Perimeter of the Convex Hull of a Plane Random Walk*, *J. Theor. Prob.* **6**, 385 (1993).
- [20] J. Randon-Furling, S. N. Majumdar, and A. Comtet, *Convex Hull of N Planar Brownian Motions: Exact Results and an Application to Ecology*, *Phys. Rev. Lett.* **103**, 140602, (2009).
- [21] S. N. Majumdar, A. Comtet, and J. Randon-Furling, *Random Convex Hulls and Extreme Value Statistics.*, *J Stat Phys* **138**, 955–1009 (2010).
- [22] G. Claussen, A. K. Hartmann, and S. N. Majumdar, *Convex hulls of random walks: Large-deviation properties*, *Phys. Rev. E* **91**, 052104 (2015).
- [23] T. Dewenter, G. Claussen, A. K. Hartmann, and S. N. Majumdar, *Convex hulls of multiple random walks: A large-deviation study*, *Phys. Rev. E* **94**, 052120 (2016).
- [24] H. Schawe, A. K. Hartmann, and S. N. Majumdar, *Convex hulls of random walks in higher dimensions: A large-deviation study*, *Phys. Rev. E* **96**, 062101 (2017).
- [25] H. Schawe and A. K. Hartmann and Satya N. Majumdar, *Large deviations of convex hulls of self-avoiding random walks*, *Phys. Rev. E* **97**, 062159 (2018).
- [26] H. Schawe and A. K. Hartmann, *Large Deviations of Convex Hulls of the "True" Self-Avoiding Random Walk*



- J. Phys.: Conf. Ser. **1290** 012029 (2019).
- [27] A. K. Hartmann, S. N. Majumdar, H. Schawe and G. Schehr, *The convex hull of the run-and-tumble particle in a plane*, *J. Stat. Mech.* (2020) 053401.
- [28] S. N. Majumdar, F. Mori, H. Schawe, G. Schehr, *Mean perimeter and area of the convex hull of a planar Brownian motion in the presence of resetting*, *Phys. Rev. E* **103**, 022135 (2021).
- [29] P. Singh, A. Kundu, S. N. Majumdar and H. Schawe, *Mean area of the convex hull of a run and tumble particle in two dimensions*, *J. Phys. A: Math. Theor.* **55** 225001 (2022).
- [30] R. Eldan, *Volumetric properties of the convex hull of an  $n$ -dimensional Brownian motion*, *Electron. J. Probab.* **19**, no. 45, 1 (2014).
- [31] Z. Kabluchko and D. Zaporozhets, *Intrinsic volumes of Sobolev balls with applications to Brownian convex hulls*, *Transactions of the American Mathematical Society* **368**, 8873 (2016).
- [32] V. Vysotsky and D. Zaporozhets, *Convex hulls of multi-dimensional random walks*, *Transactions of the American Mathematical Society* **370**, 7985 (2018).
- [33] J. Kampf, G. Last and I. Molchanov, *On the convex hull of symmetric stable processes* **2012 Proceedings of the American Mathematical Society** **140** 2527–2535.
- [34] B. De Bruyne, O. Benichou, S. N. Majumdar and G. Schehr, *Statistics of the maximum and the convex hull of a Brownian motion in confined geometries*, *J. Phys. A: Math. Theor.* **55** 144002, (2022).
- [35] T. L. Snyder and J. M. Steele, *Convex Hulls of Random Walks*, *Proceedings of the American Mathematical Society* **117**, 1165 (1993).
- [36] A. Goldman, *Probability Theory and Related Fields* **105** 57–83 ISSN 1432-2064, (1996).
- [37] A. Akopyan and V. Vysotsky, *Large deviations of convex hulls of planar random walks and brownian motions*, *Ann. H. Lebesgue*, **4**:1163–1201, (2021).
- [38] V. Visotsky, *The isoperimetric problem for convex hulls and the large deviations rate functionals of random walks*, *arXiv.2306.12359*.
- [39] C. Bechinger, R. Di Leonardo, H. Löwen, C. Reichhardt, G. Volpe, and G. Volpe, *Active particles in complex and crowded environments*, *Rev. Mod. Phys.* **88**, 045006, (2016).
- [40] J. Tailleur and M. E. Cates, *Statistical Mechanics of Interacting Run-and-Tumble Bacteria*, *Phys. Rev. Lett.* **100**, 218103, (2008).
- [41] I. Santra, U. Basu, and S. Sabhapandit, *Run-and-tumble particles in two dimensions: Marginal position distributions*, *Phys. Rev. E* **101**, 062120 (2020).
- [42] L. Onsager and S. Machlup, *Fluctuations and Irreversible Processes*, *Phys. Rev.* **91**, 1505 (1953).
- [43] P. C. Martin, E. D. Siggia, and H. A. Rose, *Statistical Dynamics of Classical Systems*, *Phys. Rev. A* **8**, 423 (1973).
- [44] M. I. Freidlin and A. D. Wentzell, *Random Perturbations of Dynamical Systems* (Springer, New York, 1984).
- [45] M. I. Dykman and M. A. Krivoglaz, in “*Soviet Physics Reviews*”, edited by I. M. Khalatnikov (Harwood Academic, New York, 1984), Vol. **5**, pp. 265441.
- [46] R. Graham, in “*Noise in Nonlinear Dynamical Systems*”, edited by F. Moss and P. V. E. McClintock, Vol. **1** (Cambridge University Press, Cambridge, 1989), p. 225.
- [47] G. Falkovich, K. Gawędzki, and M. Vergassola, *Particles and fields in fluid turbulence*, *Rev. Mod. Phys.* **73**, 913 (2001).
- [48] A. Grosberg and H. Frisch, *Winding angle distribution for planar random walk, polymer ring entangled with an obstacle, and all that: Spitzer-Edwards-Prager-Frisch model revisited*, *J. Phys. A: Math. Gen.* **36** 8955 (2003).
- [49] V. Elgart and A. Kamenev, *Rare event statistics in reaction-diffusion systems*, *Phys. Rev. E* **70**, 041106 (2004).
- [50] N. Ikeda and H. Matsumoto in “*In Memoriam Marc Yor - Séminaire de Probabilités XLVII*”, edited by C. Donati-Martin, A. Lejay and A. Rouault, *Lecture Notes in Mathematics* (Springer, Cham, 2015), Vol. 2137, p. 497.
- [51] T. Grafke, R. Grauer, and T. Schäfer, *The instanton method and its numerical implementation in fluid mechanics*, *J. Phys. A* **48**, 333001 (2015).
- [52] Baruch Meerson and Naftali R Smith, *Geometrical optics of large deviations of Brownian motion in inhomogeneous media*, *J. Phys. A: Math. Theor.* **52**, 415001, (2019).
- [53] Tal Bar and Baruch Meerson, *Geometrical optics of large deviations of Brownian motion in inhomogeneous media*, *J. Stat. Mech.* (2023) 093301.
- [54] U. Villanueva-Alcalá, J. R. Nicolás-Carlock, D. Boyer, *Diffusion limited aggregation, resetting and large deviations of Brownian motion*, *Mol. Phys.* e2276906, (2023).
- [55] A. Hehl, *The Isoperimetric Inequality*, <https://www.math.uni-tuebingen.de/ab/GeometrieWerkstatt/IsoperimetricInequality.pdf>.
- [56] J. Weigert, *The Sagacity of Circles: A History of the Isoperimetric Problem - The Work of Jakob Steiner*, *MathDL, MAA*, (2006).
- [57] T. Agranov, B. Meerson, and A. Vilenkin, *Survival of interacting diffusing particles inside a domain with absorbing boundary*, *Phys. Rev. E* **93**, 012136 (2016).
- [58] F. Di Trapani, T. Franosch, and M. Caraglio, *Active Brownian particles in a circular disk with an absorbing boundary*, *Phys. Rev. E* **107**, 064123 (2023).
- [59] S. A. Iyaniwura, Z. Peng, *Asymptotic analysis and simulation of mean first passage time for active Brownian particles in 1-D*, *arXiv:2310.04446*.
- [60] R. J. Harris and H. Touchette, *Current fluctuations in stochastic systems with long-range memory*, *J. Phys. A: Math. Theor.* **42**, 342001 (2009).
- [61] R. J. Harris, *Fluctuations in interacting particle systems with memory*, *J. Stat. Mech.* (2015) P07021.
- [62] R. L. Jack, *Large deviations in models of growing clusters with symmetry-breaking transitions*, *Phys. Rev. E* **100**, 012140 (2019).
- [63] R. L. Jack and R. J. Harris, *Giant leaps and long excursions: Fluctuation mechanisms in systems with long-range memory*, *Phys. Rev. E* **102**, 012154 (2020).
- [64] T. Agranov and G. Bunin, *Extinctions of coupled populations, and rare event dynamics under non-Gaussian noise*, *Phys. Rev. E* **104**, 024106 (2021).
- [65] N. R. Smith, O. Farago, *Nonequilibrium steady state for harmonically-confined active particles*, *Phys. Rev. E* **106**, 054118 (2022).
- [66] F. Bouchet, R. Tribe and O. Zaboronski, *Sample-path large deviations for stochastic evolutions driven by the square of a Gaussian process*, *Phys. Rev. E* **107**, 034111 (2023).
- [67] N. R. Smith, *Nonequilibrium steady state of trapped active particles*, *Phys. Rev. E* **108**, L022602 (2023).
- [68] D. S. Dean, S. N. Majumdar, and H. Schawe, *Posi-*

- tion distribution in a generalized run-and-tumble process*, [Phys. Rev. E \*\*103\*\*, 012130 \(2021\)](#)
- [69] P. Pietzonka, K. Kleinbeck and U. Seifert, *Extreme fluctuations of active Brownian motion*, [New J. Phys. \*\*18\*\*, 052001 \(2016\)](#).
- [70] C. Kurzthaler, C. Devailly, J. Arlt, T. Franosch, W. C. K. Poon, V. A. Martinez, and A. T. Brown, *Probing the Spatiotemporal Dynamics of Catalytic Janus Particles with Single-Particle Tracking and Differential Dynamic Microscopy*, [Phys. Rev. Lett. \*\*121\*\*, 078001 \(2018\)](#).
- [71] U. Basu, S. N. Majumdar, A. Rosso, and G. Schehr, *Long-time position distribution of an active Brownian particle in two dimensions*, [Phys. Rev. E \*\*100\*\*, 062116, \(2019\)](#)
- [72] Our coefficient  $\pi/4$  in Eq. (52) appears to be equal to half the coefficient 1.56 that was numerically observed in Fig. 5(a) of Ref. [24] (the factor of one half comes from their choice of  $D = 1/2$ ). Similarly, the coefficient 5.3 that we inserted in Eq. (53) equals half the coefficient 10.61 that was numerically observed in Fig. 5(c) of Ref. [24].